GEOSTATISTICALLY MODELING TOPOGRAPHICALLY-CONTROLLED DEPOSITION OF SUB-SEISMIC SCALE SANDSTONE PACKAGES WITHIN A MASS TRANSPORT DOMINATED DEEP-WATER CHANNEL BELT

Lisa Stright[1], Anne Bernhardt[1], and Alexandre Boucher[2]

[1]*Department of Geological and Environmental Sciences, Stanford University, Stanford, CA, 94305 USA*

[2]*Consulting Professor in the Department of Environmental Earth System Science, Stanford University, Stanford,* CA, 94305 USA

ABSTRACT

The irregular surface topography of subaqueous mass-transport-deposits (MTDs) plays a primary role in controlling the deposition of sand from turbidity currents in the vicinity of the Puchkirchen field in the Molasse Basin, Upper Austria. The MTD topography created mini-basins in which sandstone reservoirs accumulated. These accumulations are difficult to laterally correlate using well-log data due to variable and unpredictable shape and size. Prediction is further complicated because the sandstone accumulations are difficult to detect in seismic-reflection data. Geostatistical modeling methods, which provide a framework to characterize spatial uncertainty, have focused on channel-levee-overbank-lobe models in deep-water depositional settings, which do not apply in this case. To overcome these challenges related to the lack of reliable lateral prediction methods, a new geostatistical modeling approach is presented.

We introduce a methodology to stochastically model sandstone accumulations whose irregular shape is defined by the underlying topography of the upper surface of one or multiple MTD(s). The modeling process simulates debris flow lobes followed by turbidites that fill in the accommodation space

between debris flow lobes. Extensive data analysis is first performed to understand the extent to which available seismic attributes can aid in interwell prediction of the presence or absence of each of the defined depositional facies, as well as their geometries and distributions. We then present a modeling approach by which each successive depositional body is modeled constrained to 1) preceding topography, 2) seismic attributes, and 3) well data.

INTRODUCTION

Irregular surface topography of subaqueous mass-transport-deposits (MTDs) have been documented in high-resolution shallow seismic-reflection data (e.g., Hampton et al. 1996; Normark et al. 2004), deeper subsurface seismic-reflection data (e.g., Moscardelli et al. 2006; Garziglia et al. 2008; Hubbard et al. 2009), and outcrop studies (Pickering and Corregidor, 2005; Shultz et al., 2005; Armitage et al., 2009). The irregular nature of these surfaces is important because it often plays a primary role in controlling the deposition of sand from turbidity currents. The bed scale products and relationships between these two end-member deep-water depositional processes have been observed in outcrop (Armitage et al. 2009, Jackson and Johnson, 2009). These authors put forth the hypothesis that the topography from MTDs act to deflect turbidity currents, causing a loss of turbulence and deposition of sand. Not only are these sandstone accumulations interesting from a process sedimentology standpoint, they are also important petroleum explorations targets. Recent work by Bernhardt et al. (this volume) has documented similar relationships between sandstone and MTDs in the subsurface of the Molasse Basin, highlighting potential stratigraphically trapped sandstone accumulations.

To date, more than 40 gas fields have been discovered and close to 700 wells drilled, with new gas fields still being discovered in the Molasse Basin (de

Ruig and Hubbard, 2006). Many of the discoveries have been broad, low-relief combination structural/stratigraphic traps within the channel belt, similar to the Puchkirchen field. The current exploration targets in the channel belt are subtle stratigraphic traps. In and around the Puchkirchen gas field these are MTD-topography-controlled sandstone accumulations. Prediction of such accumulations is complicated because the minimum resolvable scale of the seismic-reflection data in the basin is approximately 30 m. This limited resolution makes it difficult to 1) determine the topography of upper surfaces of MTDs, and 2) detect sandstone accumulations, which are 1-20 m thick. Furthermore, the MTD topography produces mini-basins for sandstone accumulations that are unpredictable in shape and size. Lateral correlation of reservoir units using well-log data is difficult and a correlation is commonly established by comparing pressure data between wells (de Ruig and Hubbard, 2006). The presence, quality and distribution of the sealing facies is also critical to stratigraphic trap definition, but is not the focus of this work. To overcome challenges related to the lack of reliable lateral prediction methods, a geostatistical modeling approach is presented.

Geostatistical modeling can provide alternative realizations[1] (using one model) or a probability (averaging multiple models) of encountering a sandstone reservoir. Development of models for deep-water depositional systems has focused on either sinuous channels that are levee or erosionally confined (Caers et al., 2003; Liu et al., 2004; Larue and Hovadik, 2006; Labourdette et al., 2007; Pyrcz et al., 2008; Zhang et al., 2009) or basin-floor or overbank lobes associated with loss of confinement from sinuous channels (Pyrcz et al., 2005; Wellner et al., 2006). These models have limited applicability in the vicinity of the Puchkirchen

[1] A realization is a possible representation of the reservoir as parameterized by the stochastic model

field because sandstone deposition is controlled by MTD surface topography and not sinuous channel morphologies. As a result, the shape, size and location of sandstone accumulations are difficult to predict. Therefore, predicting the location of deposition and resulting topography of debris flow lobes becomes an important part of the modeling process and reservoir seal prediction. Moreover, given that the sandstone bodies are below seismic resolution limits, modeling the geometries of the non-reservoir components, which are better resolved by seismic attributes, can provide a pathway to modeling sandstone bodies.

In this paper we present a methodology to stochastically model sandstone accumulations whose irregular shape is defined by the underlying topography of the upper surface of one or multiple MTD(s). Extensive data analysis is first performed to understand the extent to which the available seismic attributes can aid in the interwell prediction of the presence or absence of each of the defined facies, as well as describe their geometries and distributions. We then present a modeling approach by which each successive depositional body is modeled constrained to 1) preceding topography, 2) seismic attributes, and 3) well data.

GEOLOGIC SETTING AND PREVIOUS WORK

The Tertiary Molasse Basin is a classical asymmetric foreland basin, which contains a thick succession of deep-water sediments (de Ruig and Hubbard, 2006). De Ruig and Hubbard (2006) used RMS amplitude maps from regional 3D seismic-reflection data, wireline log and core data to develop a geological model for the deep-water deposits of the Upper Austrian Molasse. Their work highlighted a west- to east–trending basin confining an axial deep-water channel belt (3-6 km wide by >100 km long) that runs subparallel to the Alpine thrust front (Fig. 1a). They described and interpreted depositional elements within the basin; channel belt, overbank wedge, overbank lobe, and tributary-channel and slope-fan deposits. Hubbard et al. (2009) analyzed cores and wireline logs from hundreds of wells, and correlated them with the 3D seismic-reflection data set throughout the Molasse Basin. Based on their observations within the channel belt, they interpreted the bed-scale processes associated with turbidity currents and developed a model to explain facies distribution. Their model depicts an organized inner channel, levee and overbank deposition confined by the larger channel belt margins.

Bernhardt et al., (this volume) refined the model presented by Hubbard et al. within the vicinity of the Puchkirchen field. The model was based on bed-scale interpretation of more than 300 m of sediment core, logged on a centimeter scale combined with interpretation of facies proportion models from Stright et al. (2009). Stright et al. (2009) created a multi-attribute, multi-scale (MA-MS) well-to-seismic calibration to derive facies proportions from inverted seismic attributes, P-impedance and Vp/Vs ratios, based on well log predicted facies validated from core descriptions. Supplemental calibration points were generated from a data-driven Markov-chain based on statistics extracted from wells logs. The proportion of a facies is defined as the percentage of each defined facies within a single seismic voxel (25 m bin size and 4 ms vertical sample rate). These facies proportion prediction volumes are data-driven observations of seismic and sub-seismic scale features that directly relate the underlying lithofacies to seismic attributes.

Bernhardt et al. (this volume), results show that in the vicinity of the Puchkirchen field, sedimentation is largely dominated by debris flow mudstone and conglomerate and, to a lesser extent, turbiditic sandstone. They observed a vertical relief of debris flow mudstone topography that is consistent with the maximum thickness of turbiditic sandstone accumulations and, based on these observations, interpreted the control of sandstone deposition as a MTD-topography-dominated (Fig. 2). The refined model describes mass transport processes depositing large debris flow build-ups in the form of levees and lobes, which partially or fully fill the width of the channel belt. Succeeding turbidity currents deposit significant amounts of sand preferentially behind these build-ups, within debris flow mini-basins, and in local topographic lows on top of debris flow deposits.

DATA

A wealth of core, well log and seismic data from the Puchkirchen Field lends itself well to an extensive geostatistical study to address the difficult task of predicting sub-seismic, stratigraphically trapped reservoir sandstone (Fig. 1b). More than fifty wells have been drilled in and around the Puchkirchen Field, all of which have been logged with a standard suite of wireline logs; spontaneous potential (SP) or gamma ray (GR), sonic (DT) and resistivity. Greater than 330 m of core have been sampled in thirteen wells through reservoir and non-reservoir intervals. 3D seismic-reflection data covers the Puchkirchen field and a significant portion of the Molasse Basin (Fig. 1a). It has been pre-stack time migrated, filtered to 14-102 Hz and automatic gain control scaled with a 1500 ms window. The dominant frequency is 28 Hz and the average velocity is 2800 m/s which results in a maximum theoretical resolution of 33 m. A simultaneous inversion (Russell et al. 2006) completed by HOT Engineering (2008), generated P-impedance, S-impedance and density volumes in a near-field exploration project (Fig. 1c). There is an adequate match between the P-Impedance volume and P-Impedance logs calculated in two wells with dipole sonic (location of wells shown in Fig. 1b). The S-Impedance also shows an adequate match, however, the resulting volume is significantly noisier than the P-Impedance volume.

DATA ANALYSIS: METHODOLOGY

The first step in the modeling process is to perform a thorough data analysis to elucidate 1) what facies can or cannot be predicted from which seismic attributes, 2) the distributions of sizes and geometries of geobodies, and 3) vertical and lateral stacking relationships between geo-bodies. The first point is extensively addressed in this paper. Points two and three are extracted from the work presented in Bernhardt et al. (this volume).

Measurement error, noise and limited bandwidth provide an inexact relationship between facies and seismic attributes. First, to capture this inexact relationship, the seismic attributes are cast into a probabilistic framework. That is, instead of analyzing whether high amplitude is conglomerate, we analyze a conditional probability, $P(A|D)$, where $P(A|D)$ is the probability of encountering conglomerate (A) given high amplitude (D).

These conditional probabilities are generated with Bayesian classification using Baye's theory:

$$P(A|D) = P(D|A)P(A)/P(D)$$

where A = facies class [ss, ms/ss, dms, cgl]

D = seismic attribute

$P(D|A)$ is a distribution of D where A exists, for example, all of the values of amplitude where conglomerate is present. This conditional probability is obtained via calibration of facies logs defined in the well and collocated seismic attributes. $P(A)$ is the overall proportion of the facies A and $P(D)$ is the probability that the value of D is encountered. Once $P(D|A)$, $P(A)$ and $P(D)$ are captured at the well locations, the calibration is used to predict $P(A|D)$ away from well locations. An in-depth discussion regarding Bayesian classification of rock types using seismic attributes can be found in Avseth et al. (2005).

The process of generating conditional probability models is depicted in Figure 3 and described in the following steps:

1. A facies log is generated at every well using a neural network validated with core descriptions (refer back to Stright and Bernhardt, SPODDS volume 2008; Fig. 3A, log track 1).

2. Seismic attributes are extracted along the well traced from the seismic volume (Fig. 3A, log track 2)

3. Histograms of the value of the seismic attribute are generated for each facies category, P(D|A). Examples of a good calibration, the bad calibration, and realistic calibration are shown in Fig. 3B--D, respectively.

4. These calibration curves are used in an inverse manner to generate facies probability cubes throughout the entire 3-D seismic volume, away from well control, P(A|D). Example probability traces generated using this Bayesian classification are shown in Figure 3A, log track 3.

Based on this simplified example, the worst-case scenario provides a 3-D estimation where each facies is equally probable at each seismic sample location. In this worst-case scenario the seismic attribute does not provide any aid to facies prediction. On the contrary, in the best-case scenario, the seismic attribute provides perfect information for facies prediction. In practice, the seismic attribute contributes smooth, low-resolution information that provides high probabilities of or predicting large homogeneous facies packages and lower probabilities of predicting smaller or mixed facies packages.

Once the models are generated, they are used to answer two critical questions: 1) Do seismic attributes predict certain facies better than others? and, 2) which seismic attributes are better at predicting the facies of interest? The second step is to analyze the conditional probability predictions generated from each seismic attribute to address these questions (ref. Fig. 4). This validation step extracts facies probabilities generated with the Bayesian classification at each location and compares probabilities to existing facies in those wells. As a visual tool, a modified box and whisker plot is used (McGill et al., 1978) to analyze the quality of the seismic attribute. Box plots provide a simplified way to analyze and compare multiple data distributions. Figure 4A presents the box plot and describes each component of the plot. The lowest whisker and the highest whisker are the P10 and P90 of the distribution, respectively. The left and the right extents of the box are the P25 and P75 of the distribution, respectively. Finally, the median (or P50) is shown by a bold vertical line and the mean by a lighter weight vertical line capped with triangles. The P10, P25, P50, P75 and P90 are all extracted from a cumulative distribution of the data.

Two boxes are shown on each plot: the probability of misclassification ($P(A|D)$ when A is not present, cross-hatch fill) and the probability of correct classification ($P(A|D)$ when A is present, solid fill). To analyze the reliability of a seismic attribute to predict a given facies (i.e., is the probability of correct classification greater than the probability of misclassification), the relationships between these two boxes and their means can be studied. To assess the spread between correct classification and misclassification, the difference in the mean values of the two distributions is used (Zhu and Journel, 1993; Goovaerts, 1997). This difference will be referred to as $\Delta\mu$. When the probability of correct classification is close to 1.0 and the probability of misclassification is close to 0.0, the boxes are far apart and the difference in means is close to 1.0 ($\Delta\mu$ ~= 1.0). For this case, the seismic attribute provides perfect information in predicting a given facies. When the probability of correct classification is approximately the same as the probability of misclassification, the boxes overlap and the difference in means is close to 0.0 ($\Delta\mu$ ~= 0.0). In this case, the seismic attribute contains no information to help in predicting a given facies. Finally, the worst-case scenario occurs when the probability of misclassification is greater than the probability of correct classification ($\Delta\mu < 0.0$), and the seismic attribute will consistently be misclassified as the wrong facies. The realistic case generally exists somewhere between perfect information and no information (Fig. 4B).

Although the difference in the means is a way to measure the strength of the relationship between the facies and the seismic attribute, it is also critical to analyze the difference in the medians (ΔP50). The mean is highly influenced by skewed distributions. In seismic attributes the data do not have sharp changes at bed boundaries and the edges of blocky facies profiles are smoothed causing the distributions to become skewed. Therefore, a large difference in the median values provides information on the skewed distributions particularly if the difference between the mean values is small. In the following results, both the difference in the mean ($\Delta\mu$) and median (ΔP50) is presented.

DATA ANALYSIS: RESULTS

Measuring the success of a single seismic attribute in predicting facies

Facies Interpretation from Amplitude

While it is often straightforward to interpret large-scale depositional packages from seismic-reflection amplitudes on the basis of amplitude brightness and reflector continuity, specifically linking an amplitude signature directly to an underlying facies is often ambiguous. For example, an amplitude map through the Puchkirchen field interval (Fig. 5), presents the question: which amplitudes represent reservoir sandstone accumulations? It is often tempting to associate high amplitudes, in the case of the Puchkirchen formation, with coarse-grained channel belt deposits (e.g., conglomerate). How reliable is this association and is it possible to be more specific?

To evaluate the reliability of such an association, the seismic-reflection volume was phase-rotated 90 degrees such that amplitude signatures could be correlated with layer properties instead of layer boundaries. The distribution of facies by amplitude, $P(D|A)$, used to generate probability cubes is shown in Figure 6a and the box plots of $P(A|D)$ is shown in Figure 6b. In these plots, the "high" amplitudes are quite ambiguous and none of the $\Delta\mu$ values are greater than 20%, placing amplitude in the statistical range of "no information". The best correlation is between conglomerate and disturbed mudstone and amplitude, although the probability of a correct classification is skewed toward the probability of a misclassification because the medians are closer than means. There are very few locations where facies is correctly predicted from amplitude, in all cases there is less than 50% probability of making the correct classification.

This is not surprising because amplitudes are strongly influenced by impedance contrasts from beds above. Reflector strength and continuity is more powerful for large-scale horizon interpretations. A seismic inversion sharpens boundaries, reduces noise, enhances resolution by removal of the wavelet effect, and converts relative impedance contrasts to absolute impedance contrasts (Coléou et al., 2003). In short, an inversion can provide impedance values that can be better utilized for lithology prediction.

Simultaneous Inversion Attributes (P-impedance, S-Impedance, Vp/Vs)

The potential of reservoir prediction directly from P-impedance and Vp/Vs for the Puchkirchen formation is illustrated in Figure 7a, a cross-plot of

Vp/Vs versus P-impedance from well log samples (15 cm sample rate). The rock physics template, which is a combination of the soft sediment model for shale and the constant cement model for the sand (Avseth et. al, 2005), is shown. The high impedance values are primarily aligned with conglomerate. Mudstone is a low impedance facies and is difficult to differentiate from reservoir sandstone, interbedded sandstone and mudstone, and soft, organic rich shale based only on P-impedance. This is due to a weak acoustic contrast and sub-seismic scale thickness. The addition of Vp/Vs shows a strong delineation of facies over simply using P-impedance alone. The Vp/Vs ratio reveals a more distinct sandstone signature pointing to using both acoustic and elastic inversion attributes for predicting facies. However, these delineations are at the well log scale, and much of this differentiation is lost when the data is filtered to a lower resolution by the seismic wavelet. The MA-MS (multi-attribute, multi-scale; see Stright et al., 2009) cross-plot (Fig. 7b) reveals the difficulty of predicting individual lithologies at the seismic scale. The thin sandstone beds are incorporated into the seismic signal of the surrounding beds and are no longer differentiated by the seismic attributes (Fig. 7a). Furthermore, a given pair of seismic-scale P-impedance and Vp/Vs may contain different proportions of facies, revealing the probability of proportions and the non-uniqueness of the inverse problem.

The box plots (Fig. 8) shows that P-Impedance from seismic inversion provides a stronger prediction of disturbed mudstone and conglomerate than amplitude, and the probability distributions are now skewed toward correct classification rather than misclassification. Conversely, P-Impedance provides no information for predicting sandstone and interbedded sandstone and mudstone (i.e., very low $\Delta\mu$). S-impedance shows a similar result, while Vp/Vs does not appear to provide a reliable prediction of any of the facies. Figure 7 shows that a low Vp/Vs ratio should at least differentiate sandstone, even at the seismic scale. The low reliability of classification is likely due to the sub-seismic scale nature of the sandstone beds.

Measuring the success of multiple seismic attributes in predicting facies

While each of the individual attributes from the seismic inversion may not be able to predict each facies if they are taken independently, a combination of attributes is expected to (refer back to Fig. 7). A conditional probability of facies given all of the seismic attributes, P(SS|Ip, Is, Vp/Vs), can be explicitly inferred from a 3D cross-plot of the data (cf. Avseth et al., 2005). However, this approach assumes independence of each of seismic attributes. There is likely some data redundancy in the seismic attributes (i.e., Vp/Vs is calculated from Ip and Is as Ip/Is). If Vp/Vs derived from these two attributes, is it redundant or does it bring new information? For example, if Ip and Vp/Vs both reveal a high probability of encountering sandstone, is this more information and should a combined probability should reflect a higher joint probability? If there is conflicting information from these sources, what then should be the joint probability.

Recent models have been introduced which take into account data redundancy and provide a framework for combining each of the individual conditional probabilities into a single conditional probability (Tau model from Journel, 2002; Nu model from Polyakova and Journel, 2007). For this study, the Nu model was used with a data redundancy factor of 1. The result is a combined P(SS|Ip), P(SS|Is), and the P(SS|Vp/Vs) into a single probability model of P(SS|Ip, Is, Vp/Vs), accounting for the redundancy of information in the seismic attributes. The result of combining the individual probabilities into one probability model strengthens the prediction of disturbed mudstone and conglomerate from the seismic attributes, but also sandstone. Conversely, interbedded sandstone and mudstone is less reliably predicted because it is of such a low proportion, the beds are quite thin, and the multiple sources of information have removed some of the ambiguities in prediction.

Up to this point, the discussion has focused on the probability of a correct classification. It is also quite important to discuss the penalty of being wrong. That is, when the prediction is wrong, what wrong facies was predicted instead of the correct one? For this, we will look at the confusion matrix (Fig. 9b). The diagonal of the matrix reveals the probability of predicting the "right" facies with the Bayesian classification. The off-diagonal elements show which facies is most likely to be predicted when the "right" one isn't predicted. For example, only 40% of the time sandstone will be correctly predicted, and when sandstone should be predicted and it is not, 8% of the time interbedded sandstone and mudstone will be predicted instead, while 32% of the time disturbed mudstone and 20% of the time conglomerate will be predicted instead.

Quantifying the depositional geometries: Shapes and Sizes

Based on the interpretation of the facies proportion maps large debris flows build up levees and lobes. A first order sketch of the geometry of a debris flow lobe at the point of deposition is shown in Figure 10. Additionally, from the analysis of thickness maps from the facies proportion models presented by Bernhardt et al. (this volume), a smoothed distribution of volumetric sizes of these bodies was compiled (Fig. 11). These provide a first order approximation of shapes and sizes of depositional bodies.

DATA ANALYSIS: DISCUSSION

From this extensive data analysis, it is shown that Bayesian classification of facies from multiple seismic attributes provides a more reliable classification when multiple attributes are combined taking into account the redundancy of information between each seismic attribute. Furthermore, not all facies can be reliably classified from seismic attributes. In this case, the combination of Ip, Is and Vp/Vs provide a good first order prediction of debris flow disturbed mudstone and conglomerate. Bed thicknesses of each facies are not reflected in the box plots (Figs. 8 and 9) presented herein. As the bed thickness drops below seismic resolution, there is a drop in predictability. Furthermore, as is the case with interbedded sandstone and mudstone, the low proportion of a facies detracts from predictability.

Seismic attributes are important components to guide interwell predictions. Knowledge of what the seismic attributes can reliably predict is critical in the modeling phase. This analysis has shown that the combined seismic attributes (Ip, Is and Vp/Vs) can be used to predict disturbed mudstone and conglomerate. Fortunately, the well logs and facies proportion models (Stright et al., 2009) can be leveraged to provide a finer scale prediction aid for turbiditic sandstone and interbedded sandstone and mudstone.

MODELING: METHODOLOGY

The goal of the geological modeling process is to build geocellular models that will reliably predict reservoir intervals and properties for well planning and/or fluid flow performance prediction. A typical modeling workflow will attempt to convert a geologist's conceptual image of the reservoir to a numerical representation that honors both hard (well and core) and soft (seismic and production) data collected from the reservoir. However, historically available tools such as covariance-based (2-point), Gaussian-based, geostatistical methods (cf. Goovaerts, 1997) limit the modeler's ability to include realistic interpretive geologic information into reservoir models, while Boolean object-based methods (cf. Stoyan et al., 1987) cannot match the diverse and often abundant data sampled from the reservoir interval. Furthermore, parameterization and programming of the object shapes, sizes and relationships are often difficult. Surface-based modeling algorithms (Pyrcz et al., 2005; Wellner et al., 2006) provide promise in capturing body geometries that are tied back to the sedimentological processes that generated them without the need for complex numerical solutions. At this point, it is difficult to constrain these methods to well data and seismic attributes.

Advances in training image-based modeling algorithms (Strebelle, 2000; Arpat, 2005; Zhang, 2006) have made it possible to reproduce the geometry of complex sedimentary bodies while conditioning to the diverse suite of soft (seismic) and hard (well log and core) data typically encountered in petroleum reservoirs. Training image-based modeling techniques provide the avenue to include qualitative interpretative information into reservoir models through training images, thus allowing the geologist more control to include important descriptive information. However, once again, the generation of a satisfactory training image (or images) is a challenge that geostatisticians still face.

While the training image is the basis of a shift in model building workflows, from covariance-based statistical methods toward quantitative integration of descriptive geological interpretations with field data, it is not always the appropriate tool to choose for model building. In the case of deposits around the Puchkirchen field, sandstone sedimentary bodies are irregularly shaped and cannot be placed into a training image paradigm. Therefore, a topographically-driven object-based modeling workflow is being presented. The workflow combines coarse-scale seismic attributes as local probabilities to control the placement of debris flow lobes (disturbed mudstone and conglomerate) followed by turbidity current deposition induced by uneven underlying topography (sandstone and interbedded sandstone and mudstone). The modeling workflow produces multiple alternative numerical models of sediment accumulation within the channel belt, locally constrained to facies definitions in the wells and seismic data.

Tetris

The foundation for the modeling is 1) plug-in to the Stanford Geostatistical Modeling Software (SGeMS) that generates sedimentary bodies with complex geometries, and 2) Python scripting as a command center for the simulation control. SGeMS is an open-source computer package for solving problems involving spatially related variables (Remy et al, 2009; http://sgems.sourceforge.net). It provides geostatistics practitioners with a user-friendly interface, an interactive 3-D visualization, and a wide selection of algorithms. The plug-in is in development and has been presented internally at the Stanford Center for Reservoir Forecasting Affiliates meeting (SCRF; Boucher et al., 2010). The design overcomes a major hurdle of rigidly pre-defined geological objects, and provides a framework to define complex objects from pre-coded shapes, such as ellipsoid, cuboid, kernels, or user defined shapes. These basic shapes are then combined with operations (difference, union and intersection) to create new complex shapes. For added flexibility, any shape can be translated, rotated and sheared.

Workflow

The first part of the workflow is the thorough data analysis, presented in the first part of this paper. The resulting facies probabilities obtained from a calibration between facies defined in the wells and multiple seismic attributes are the driving force for placement of the seismic-scale debris flow lobes. The shape of the debris flow lobe is depicted Figure 10. The shape is created with Tetris using the intersections between multiple spheres and ellipsoids of varying sizes. This is one possible shape for a debris flow lobe and will serve as an initial test shape for simulations.

Using all of these components (probability of debris flow lobes and debris flow lobe shapes), Python scripting is used to tell Tetris to "drop" the shapes into the model space (or grid), positioned by 1) the lowest point in the grid, and 2) a high probability from the P(disturbed mudstone, conglomerate | Ip, Is, Vp/Vs) (workflow shown in Fig. 12). Each subsequent debris flow lobe that is emplaced is draped on top of the previous topography. Once 20% of the simulation grid is filled with debris flow lobes, the simulation is paused and the result is treated as the initial topography for the next phase of modeling (Fig. 13).

In the second phase of modeling, the script controls whether a debris flow lobe or a turbidite is chosen to be simulated. The choice is made by checking how close either debris flow deposits or turbidites are to their total target proportions, and stochastically choosing one based on the distance from the target proportions. This constraint ensures that the target proportions will be met. The size of the debris flow lobe or turbidite is selected stochastically from the histogram in Figure 11. The placement of turbidites is chosen by filling the lowest topography in the grid given the stochastically selected volume of sand from the histogram. The process of simulating debris flow lobes and turbidites is repeated until the simulation grid is filled. Currently, data conditioning (or ensuring that each model matches seismic attributes and well log facies definitions) is controlled by running multiple forward models and using an accept/reject criteria that keeps the models that best fit the data and rejects the ones that do not.

MODELING RESULTS

A model from a single realization of this workflow is shown in Figure 13 showing the simulation of debris flows and turbidites with each step of the simulation. The basal topography is built by debris flow lobes and subsequent turbidite and debris flow lobe simulation generate irregularly-shaped sandstone accumulations that thin onto the debris flow build-ups in the mini-basins generated by the topography of the MTD upper surfaces.

CONCLUSIONS

We presented a detailed data analysis and proposed a modeling workflow for deposits in and around the Puchkirchen field in deep-water deposits of the Molasse basin in Upper Austria. The data analysis revealed that bringing together all of the seismic attributes from a simultaneous seismic inversion provided the best reliability for prediction of debris flow conglomerate disturbed mudstone. Conversely, deposits from turbidity currents (sandstone and interbedded sandstone and mudstone) are below seismic resolution and are not reliably classified from any individual or combinations of seismic attributes analyzed in this study.

Given this knowledge, we presented a methodology to stochastically model sandstone accumulations whose irregular shape is defined by the underlying topography of the upper surface of one or multiple MTD(s). The modeling process simulated debris flow lobes followed by turbidites that fill in debris flow lobe mini-basins. The modeling approach is constrained such that each successive depositional body is controlled by the 1) preceding topography, 2) seismic attributes, and 3) well data. This modeling process was demonstrated for the channel belt deposits in the vicinity of the Puchkirchen field.

ACKNOWLEDGEMENTS

We would like to thank Rohöl-Aufsuchungs A.G. (RAG) for financial and logistical support of our research, as well as for permission to publish their data in this study. In particular, we wish to thank Richard Derksen for his ongoing support of this research. This work has benefited greatly from discussion on petroleum geology and sedimentology with Stephan Graham, Donald Lowe and Stephen Hubbard, rock physics and seismic data interpretation with Tapan Mukerji and Gary Mavko, and geostatistical modeling with Andre Journel. We would also like to acknowledge the generous software donations from Schlumberger (Petrel) and the inversion models produced by HOT Engineering in 2009 using Hampson-Russel. Finally, valuable feedback and support has been provided by the Stanford Project on Deepwater Depositional Systems (SPODDS), an industrial affiliates program whose members include Aera Energy, Anadarko Petroleum Corporation, BHP Billiton, Chevron, ConocoPhillips, Hess Corporation, Marathon Oil Company, Nexen Energy, Occidental Petroleum, Petrobras, Reliance Industries Ltd., Rohöl-Aufsuchungs A.G. (RAG), Schlumberger and Shell.

REFERENCES

Armitage, D.A., Romans, B.W., Covault, J.A., and Graham, S.A., 2009, The influence of mass transport deposit topography on the evolution of turbidite architecture: The Sierra Contreras, Tres Pasos Formation (Cretaceous), southern Chile: Journal of Sedimentary Research.

Arpat, G.B., and Caers, J., 2007, Conditional Simulation with Patterns, Mathematical Geology, v. 39, no. 2, p. 177-203.

Avseth, P., Mukerji, T., and Mavko, G., 2005, Quantitative seismic interpretation: applying rock physics tools to reduce interpretation risk, Cambridge University Press, 359 p.

Bernhardt, A., Stright, L., and D. R. Lowe, *in preparation*, Debris Flow vs. Turbidity Current Interactions in a Large Submarine Axial Channel Belt – Puchkirchen Formation, Austrian Molasse Basin.

Boucher, A., Gupta, R., Caers, J., and Satija, A., 2010, Tetris: a training image generator for SGeMS, Stanford Center for Reservoir Forecasting (SCRF) Annual Meeting.

Caers, J., Strebelle, S., and Payrazyan, K., 2003, Interpreter's Corner—Stochastic integration of seismic data and geologic scenarios: A West Africa submarine channel saga, The Leading Edge, v. 22, no. 3, p. 192.

Coléou, T., Poupon, M., and Azbel, K., 2003, Unsupervised seismic facies classification A review and comparison of techniques and implementation, The Leading Edge, v. 22, no. 10, p. 942-953.
De Ruig, M.J., and Hubbard, S.M., 2006, Seismic facies and reservoir characteristics of a deep-marine channel belt in the Molasse foreland basin, Puchkirchen Formation, Austria, AAPG Bulletin, v. 90, no. 5, p. 735-752.
Garziglia, S., Migeon, S., Ducassou, E., Loncke, L., and Mascle, J., 2008, Mass-transport deposits on the Rosetta province (NW Nile deep-sea turbidite system, Egyptian margin): Characteristics, distribution, and potential causal processes, Marine Geology, v. 250, no. 3-4, p. 180-198.
Goovaerts, P., 1997, Geostatistics for natural resources evaluation, Applied Geostatistics Series. Oxford University Press, 483 p.
Hampton, M.A., Lee, H.J., and Locat, J., 1996, Submarine landslides, Reviews of Geophysics, v. 34, no. 1, p. 33.
HOT Engineering, G., 2007, Puchkirchen: Near Field Exploration Study, Leoben, Austria, HOT Engineering Consulting Report, 50 p.
Hubbard, S.M., Graham, S.A., and De Ruig, M.J., 2009, Confined channel-levee complex development in an elongate depo-center: Deep-water Tertiary strata of the Austrian Molasse basin, Marine and Petroleum Geology, v. 26, no. 1, p. 85-112.
Jackson, C.A., and Johnson, H.D., 2009, Sustained turbidity currents and their interaction with debrite-related topography; Labuan Island, offshore NW Borneo, Malaysia, Sedimentary Geology, v. 219, no. 1-4, p. 77-96.
Journel, A., 2002, Combining knowledge from diverse sources: an alternative to traditional data independence hypotheses, Mathematical geology, v. 34, no. 5, p. 573–596.
Labourdette, R., 2007, Integrated three-dimensional modeling approach of stacked turbidite channels, AAPG Bulletin, v. 91, no. 11, p. 1603-1618.
Larue, D., and Hovadik, J., 2006, Connectivity of channelized reservoirs: a modelling approach, Petroleum Geoscience, v. 12, no. 4, p. 291-308.
Liu, Y., Harding, A., Abriel, W., and Strebelle, S., 2004, Multiple-point simulation integrating wells, three-dimensional seismic data, and geology, AAPG Bulletin, v. 88, no. 7, p. 905-921.
McGill, R., Tukey, J.W., and Larsen, W.a., 1978, Variations of Box Plots, The American Statistician, v. 32, no. 1, p. 12.
Moscardelli, L., and Wood, L., 2008, New classification system for mass transport complexes in offshore Trinidad, Basin Research, v. 20, no. 1, p. 73-98.
Normark, W.R., Mcgann, M., and Sliter, R., 2004, Age of Palos Verdes submarine debris avalanche , southern California, Marine Geology, v. 203, p. 247-259.
Pickering, K.T., and Corregidor, J., 2005, Mass-Transport Complexes (MTCs) and Tectonic Control on Basin-Floor Submarine Fans, Middle Eocene, South Spanish Pyrenees, Journal of Sedimentary Research, v. 75, no. 5, p. 761-783.
Polyakova, E.I., and Journel, A.G., 2007, The Nu Expression for Probabilistic Data Integration, Mathematical Geology, v. 39, no. 8, p. 715-733.
Pyrcz, M.J., Boisvert, J.B., and Deutsch, C.V., 2008, A library of training images for fluvial and deepwater reservoirs and associated code, Computers & Geosciences, v. 34, no. 5, p. 542-560.
Pyrcz, M.J., Catuneanu, O., and Deutsch, C.V., 2005, Stochastic surface-based modeling of turbidite lobes, 177-191 p.
Remy, N., Boucher, A., Wu J., 2009, Applied geostatistics with SGeMS: A user's guide. Cambridge University Press, Cambridge.
Russell, B., Hampson, D., and Bankhead, B., 2006, An Inversion Primer, CSEG Recorder, v. Special Edition, no. 1, p. 96-103.

Shultz, M.R., Fildani, A., Cope, T.D., and Graham, S.A., 2005, Deposition and stratigraphic architecture of an outcropping ancient slope system: Tres Pasos Formation, Magallanes Basin, southern Chile, Geological Society, London, Special Publications, v. 244, no. 1, p. 27.

Stoyan, D., W. S. Kendall, and J. Mecke, 1987, Stochastic geometry and its applications: New York, John Wiley & Sons, 345 p.

Strebelle, S., 2002, Conditional simulation of complex geological structures using multiple-point statistics, Mathematical Geology, v. 43, no. 1, p. 1-22.

Stright, L., and Bernhardt, A., 2008, Multi-scale rock type prediction in the Puchkirchen Formation: An approach integrating rock physics with deep-water stratigraphy and sedimentology, SPODDS Annual Meeting, 2008.

Stright, L., Bernhardt, A., Mukerji, T., Boucher, A., and Derksen, R., 2009, Revisiting the use of seismic attributes as soft data for sub-seismic facies prediction: Proportions versus probabilities, The Leading Edge, v. 28, no. 12, p. 1460-1468.

Wellner, R., Beaubouef, R., and Van, J., 2005, Jet-plume depositional bodies–the primary building blocks of Wax Lake Delta, Gulf Coast Association of Geological Societies Transactions, v. 55.

Zhang, T., Switzer, P., and Journel, A.G., 2006, Filter-Based Classification of Training Image Patterns for Spatial Simulation, Mathematical Geology, v. 38, no. 1, p. 63-80.

Zhang, X., Pyrcz, M.J., and Deutsch, C., 2009, Stochastic surface modeling of deepwater depositional systems for improved reservoir models, Journal of Petroleum Science and Engineering, v. 68, no. 1-2, p. 118-134.

Zhu, H., Journel, A.G., 1993. Formatting and integrating soft data: stochastic imaging via the Markov–Bayes algorithm. Soares Ed.., Proceedings of the 4th International Geostatistics Congress, Kluwer, Dordrecht, pp. 1–12.

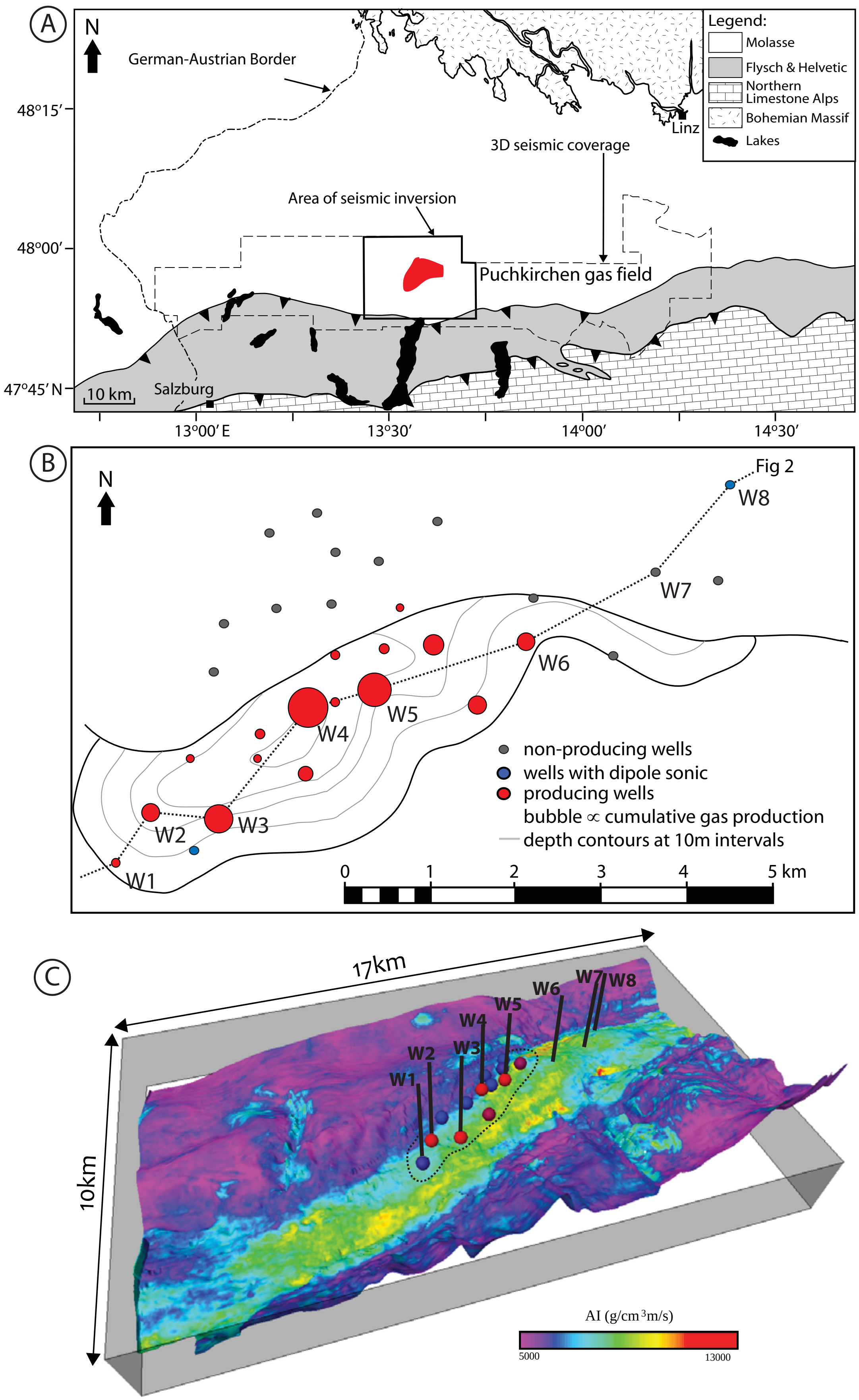

Figure 1. Basemap of the Austrian Molasse Basin and location of study area. (A) The Puchkirchen gas field location. (B) Well and cross section locations with gas production bubbles. (C) Acoustic impedance attribute shown on a stratigraphic surface. Well locations show the location of the Puchkirchen gas field (outlined), which was drilled on a structural high. Each sphere near well shows the amount of cumulative gas production, from red (high) to blue (low).

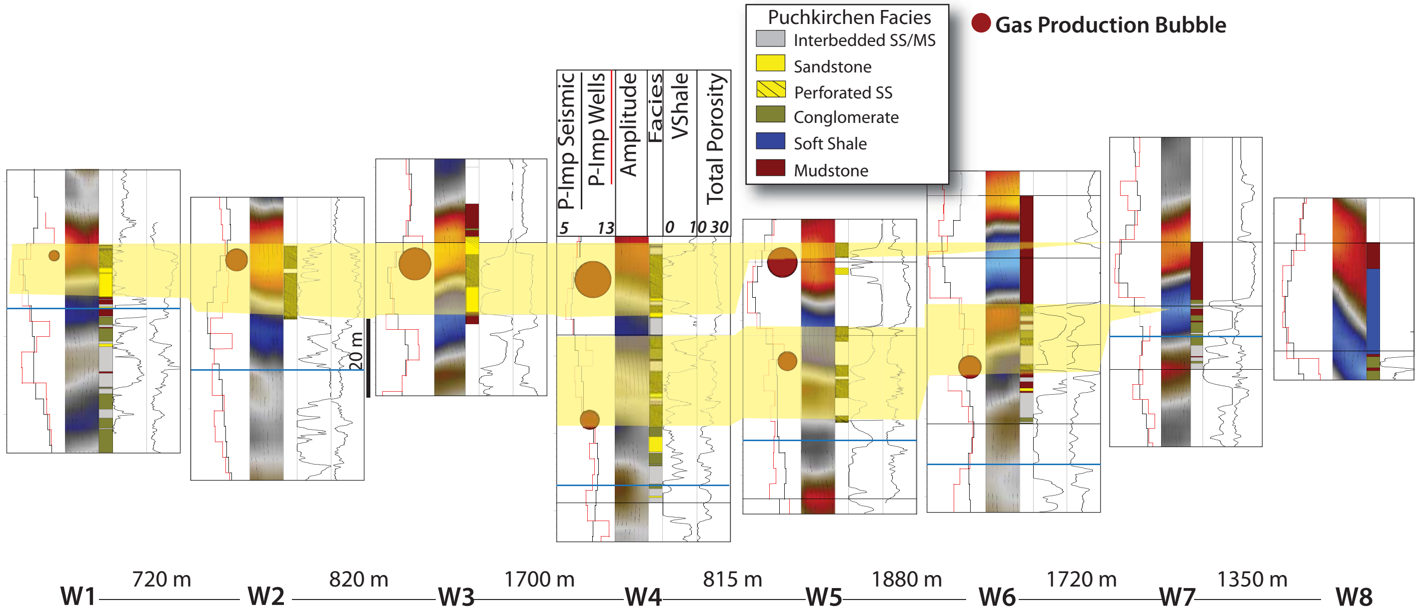

Figure 2. Well section (flattened on the Base Hall unconformity) showing the distal thinning of sandstone onto debris flow mudstone. The upper sandstone accumulation is the Puchkirchen A1 reservoir while the lower sandstone accumulation is the A2 reservoir. The seismic calibration trace is also plotted.

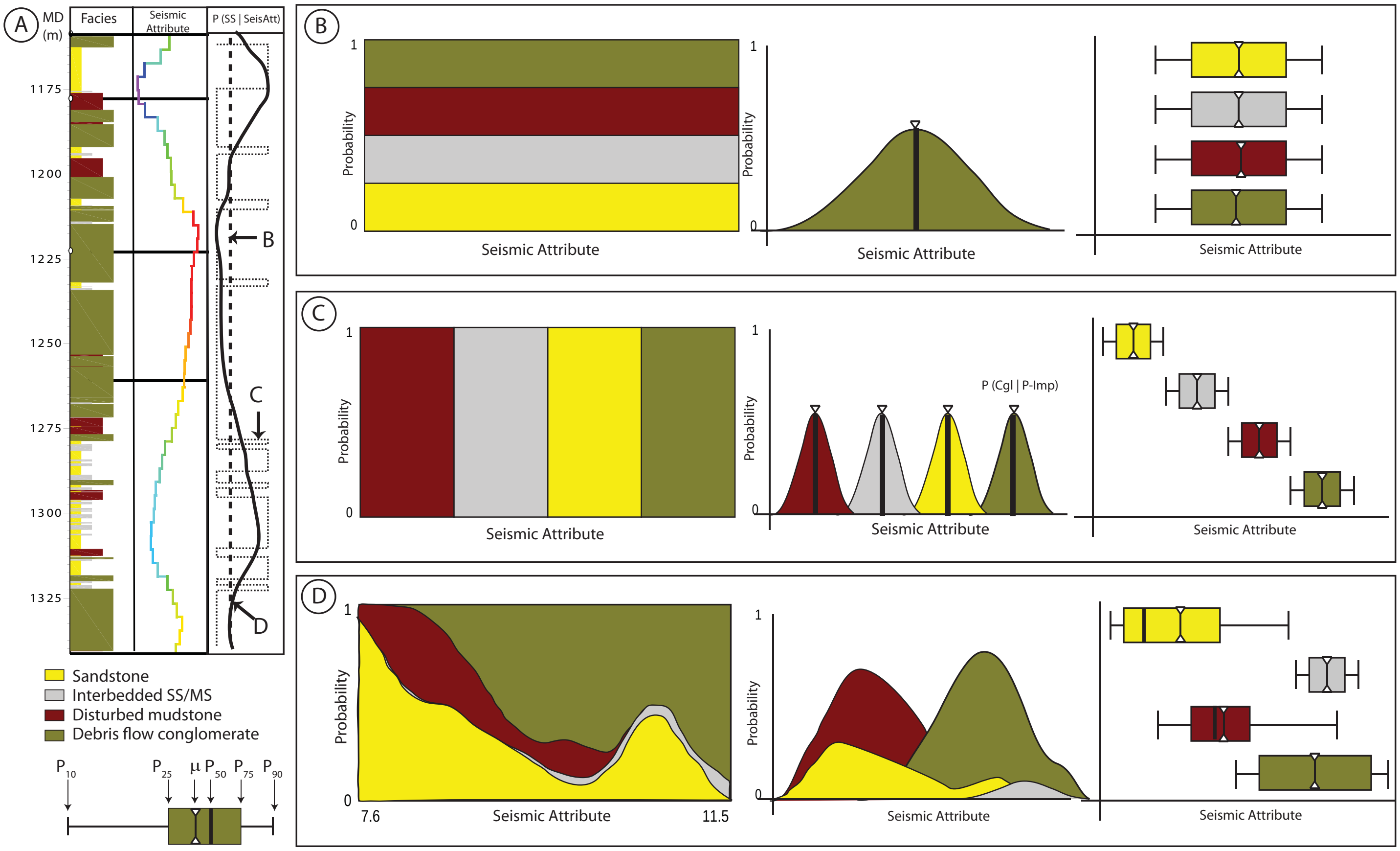

Figure 3. Conceptual depiction of how to generate a facies probability model from seismic using the Baye's classification, P(A|D) = P(D|A)P(A)/P(D). A) Well profile showing a facies log (log track 1) and corresponding P-impedance values (log track 2) from and inversion. The third log track show the probability estimations from the calibrations shown in B-D). B-D) show three different scenarios of P(D|A) from a calibration of well and seismic data where, B) the worst case scenario for probability models, C) the best case scenario, and D) a more realistic case with true data.

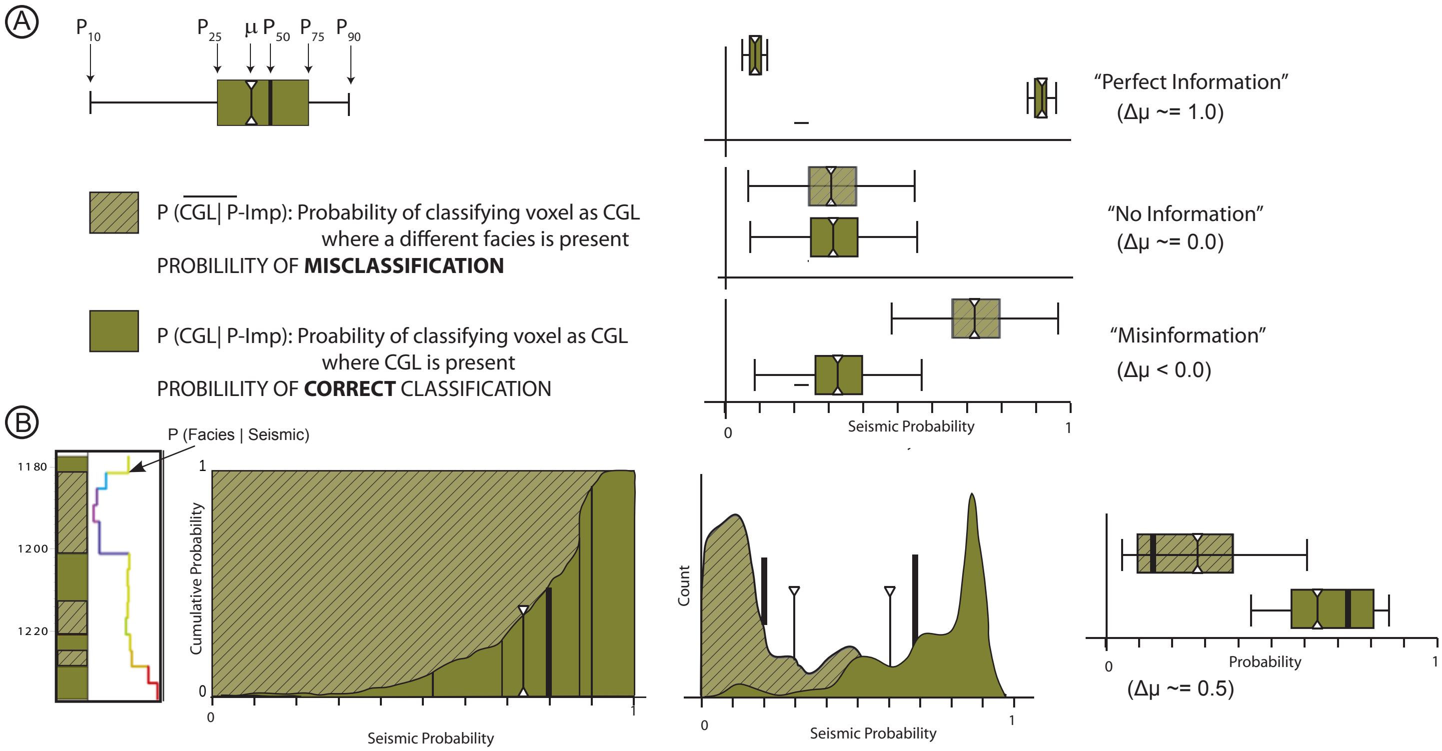

Figure 4. A conceptual diagram to understand the plots used in this paper to gauge the ability of a seismic attribute (e.g., P-Impedance) to predict a facies (e.g., conglomerate). This image is the key to interpreting the box plots presented in Figures 6, 8 and 9. We are now starting with the probability model predicting the probability of conglomerate at ever seismic voxel (Fig. 3). A) Using a well as validation we can look at how representative these probabilities are at correctly predicting conglomerate (solid fill) or misclassifying a voxel as conglomerate (cross-hatch fill). Box plots of these two probabilities reveal three cases of seismic information: 1) perfection information, 2) no information, or 3) misinformation. B) Shows a more realistic case where seismic is a relatively good predictor of conglomerate. The seismic attribute is a poor predictor when facies are interbedded at a scale finer than the seismic resolution.

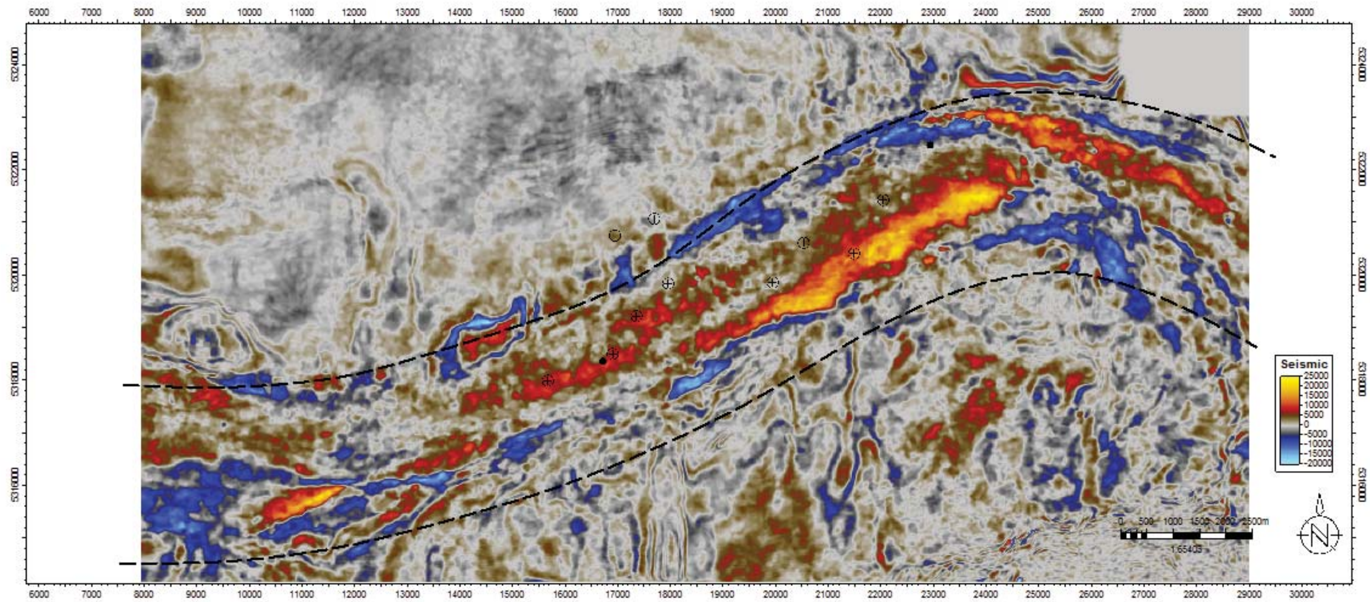

Figure 5. Instantaneous amplitude map extracted along a horizon slice that is 40 m below the reservoir horizon. The amplitude volume has been phase rotated by 90 degrees.

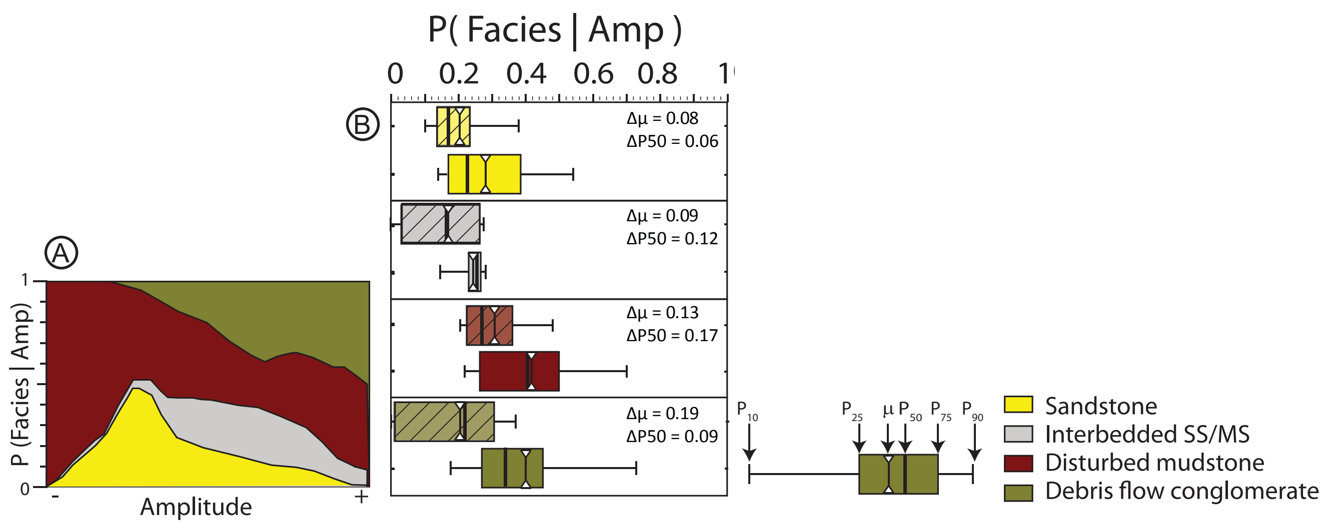

Figure 6. Box plots of the probability of predicting each facies with a phase rotated seismic amplitude (Fig. 5), P(Facies | Amplitude). The amplitude volume was phase rotated so that high and low amplitudes correspond to beds while zero-crossings correspond to boundaries. Although the amplitude map (Fig. 5) shows a strong delineation between high and low amplitude regions, there is not a direct correlation with facies because the probability of misclassification is high for all facies (i.e., Δμ and ΔP50 are low).

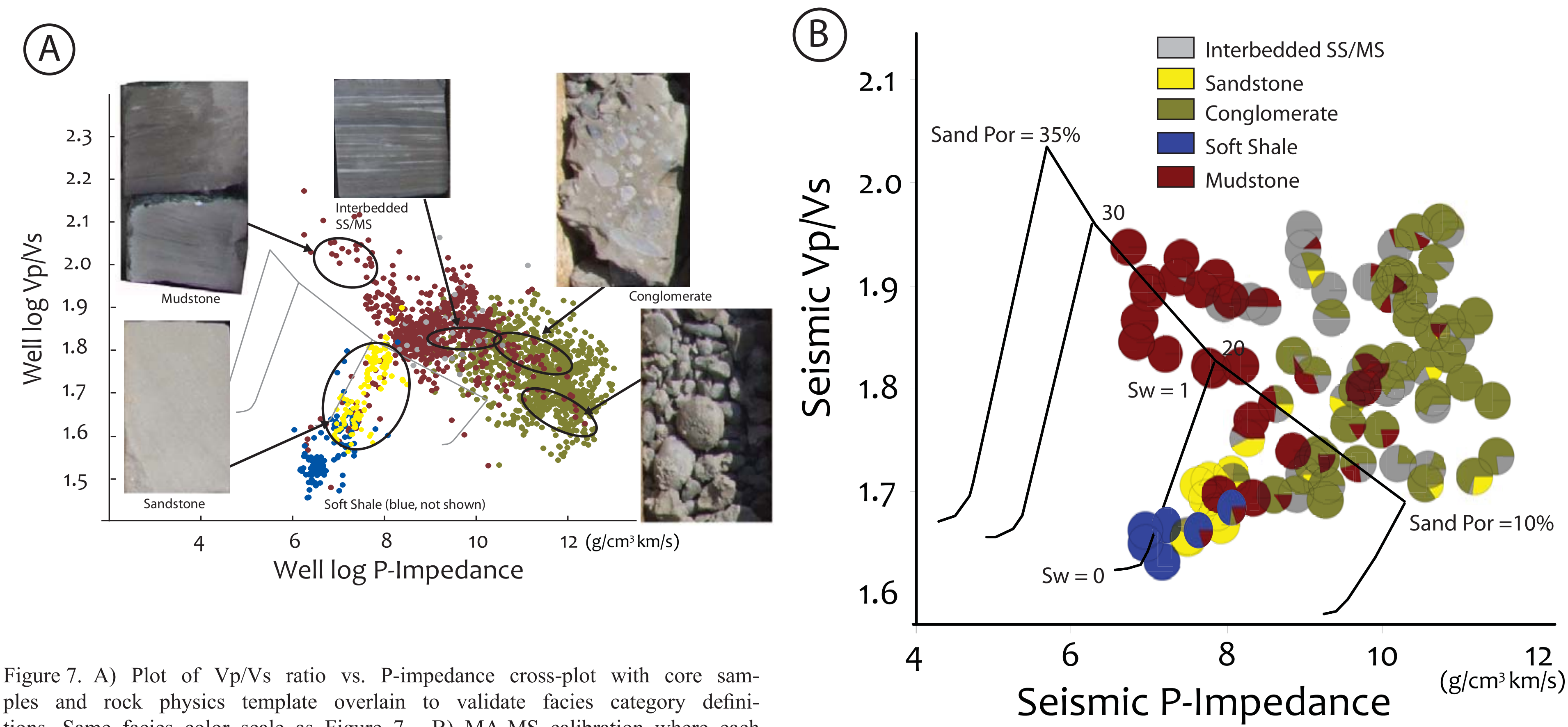

Figure 7. A) Plot of Vp/Vs ratio vs. P-impedance cross-plot with core samples and rock physics template overlain to validate facies category definitions. Same facies color scale as Figure 7. B) MA-MS calibration where each pie chart shows the fine-scale facies proportions within a seismic sample.

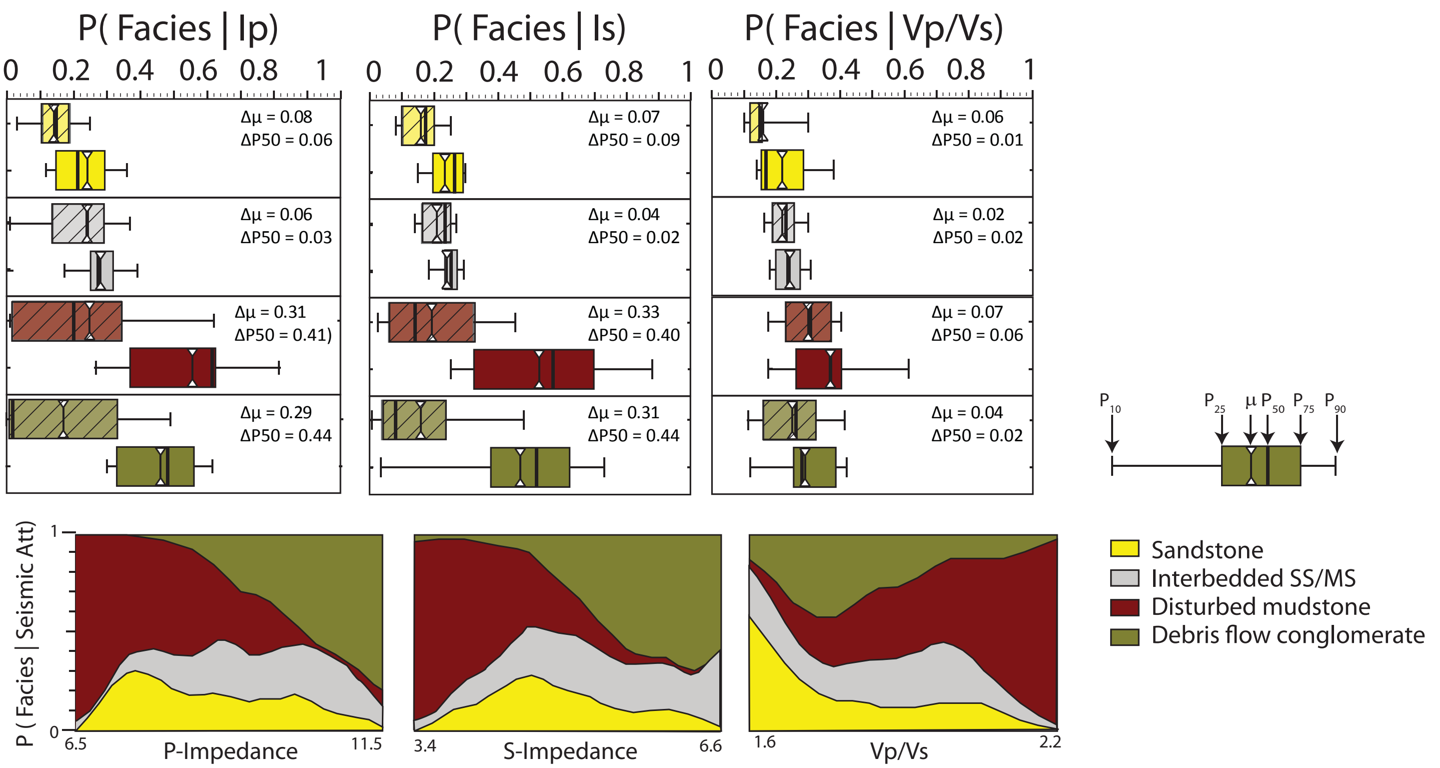

Figure 8. Box plots of the probability of predicting each facies with a seismic attributes form a simultaneous inversion, P(Facies | Ip), P(Facies | Is), and P(Facies | Vp/Vs). These plots show the individual contributions of each attribute in predicting each facies. There is a stronger correlation of disturbed mudstone and debris flow conglomerate with Ip and Is, but Vp/Vs does not reliably differentiate any of the facies alone.

A

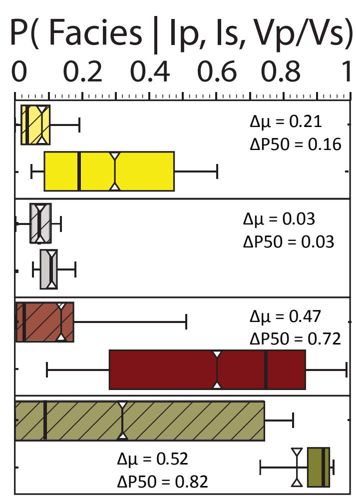

B

Nu	SS	SSMS	DMS	CGL
SS	**0.40**	0.08	0.32	0.20
SSMS	0.04	**0.20**	0.17	0.59
DMS	0.08	0.09	**0.69**	0.14
CGL	0.00	0.08	0.02	**0.90**

Figure 9. A) Box plots of the probability of predicting each facies with the combination of seismic attributes form a simultaneous inversion, P(Facies | Ip, Is, Vp/Vs). Combining the attributes generated a significantly stronger correlation of disturbed mudstone and debris flow conglomerate, while increasing the predictability of sandstone. Interbedded sandstone and mudstone is poorly predicted due to the fine-scale nature of the beds and it's overall lower proportion.

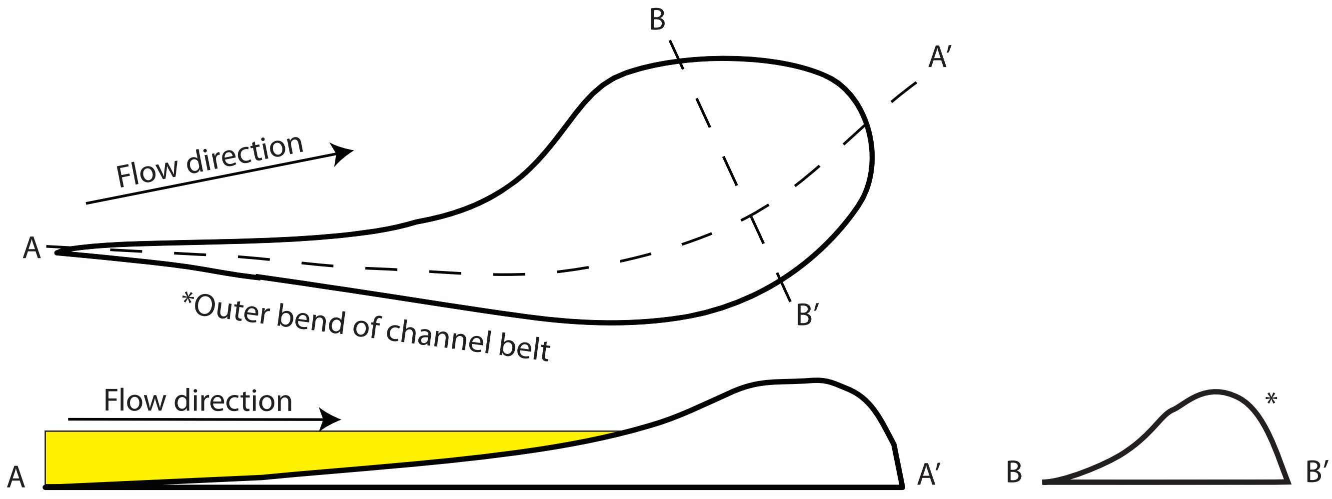

Figure 10. Diagrammatic sketch of a debris flow lobe. Section A-A' depicts the tail to snout morphology of an idealistic lobe and scenario of where sand deposition will occur behind the debris flow lobe. Section B-B' shows the preferential build-up of the lobe toward the outer bend of the channel belt.

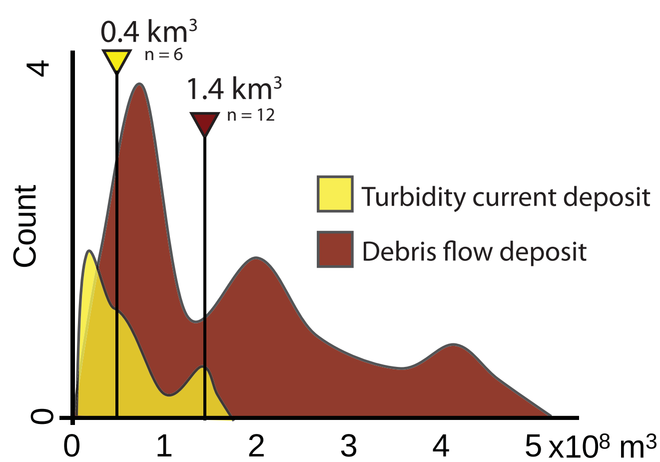

Figure 11. Distribution of the sizes (volumes) of debris flow lobes and turbidity currents measured from geobodies in Bernhardt et al. (*this volume*). Debris flow lobes are both more abundant and larger than turbidity currents. These distributions are a first -order approximation of the volumetric sizes of each gravity flow deposit to generate in the model.

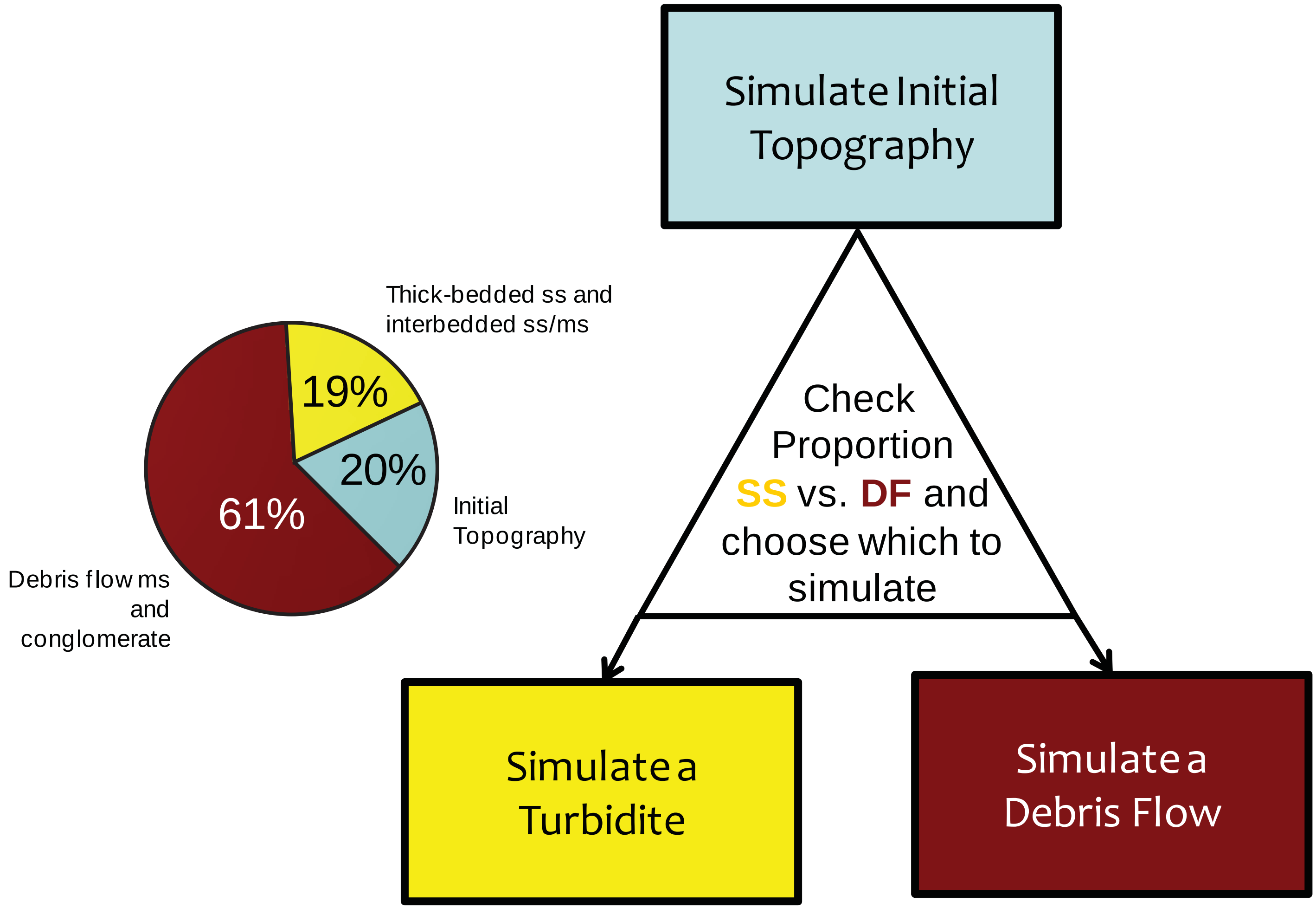

Figure 12. Workflow for simulation of sandstone accumulations in a topographically-controlled depositional system. Step 1 is to simulated an initial topography by placing debris flow lobes in the simulation grid until 20% of the grid is filled. Placement is controlled by the lowest point on the grid and the probability of debris flow from the inverted seismic attributes. Step 2 is to choose whether a turbidite or another debris flow lobe will be simulated. This is stochastically chosen depending on the proportion of debris flow and turbidite simulated previously. The process is continued until the simulation grid is filled.

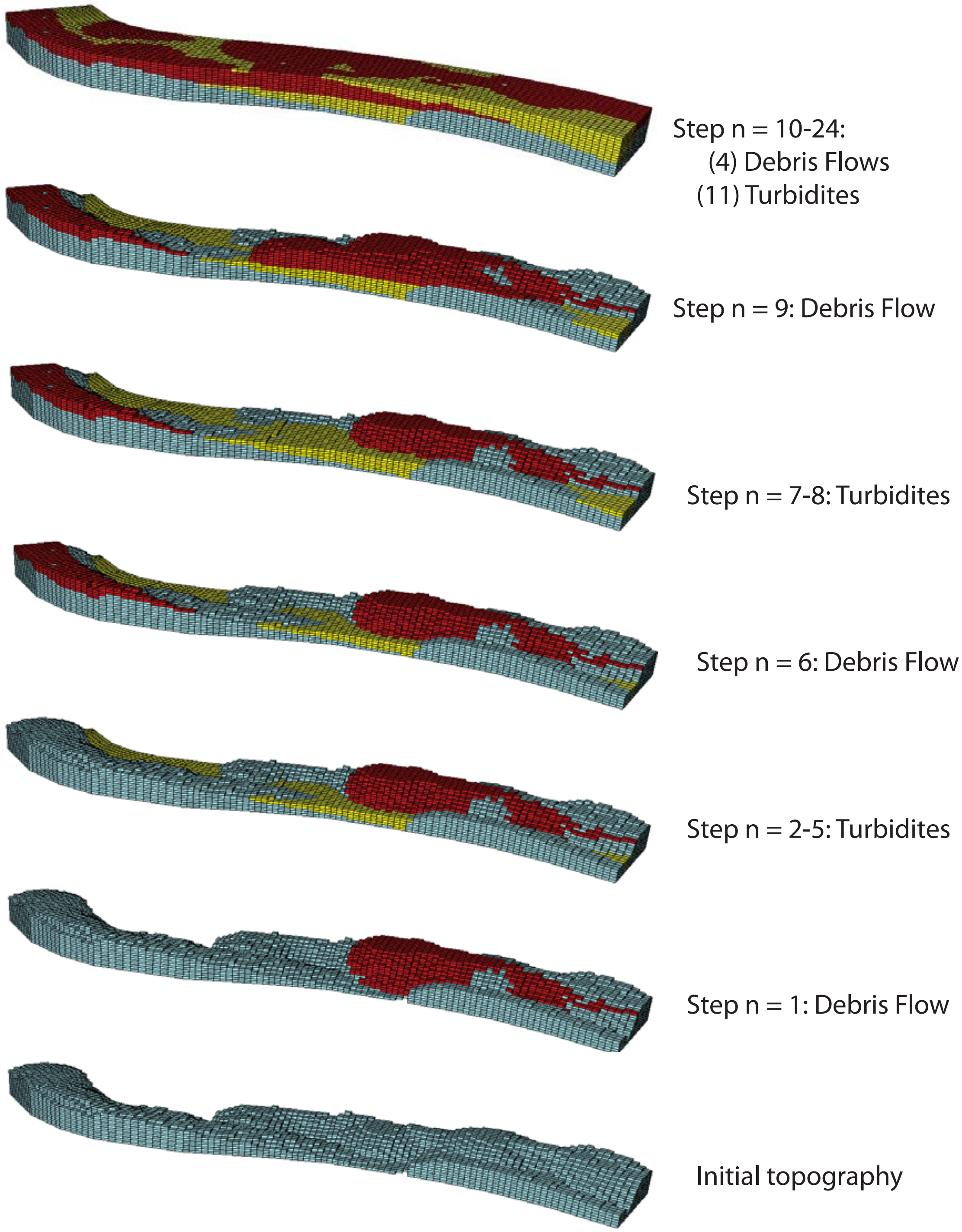

Figure 13. A model from a single realization. The base topography (light blue) is built with debris flow lobes and subsequent turbidite (yellow) and debris flow lobe (red) simulation generate irregularly-shaped sandstone accumulations that thin onto the debris flow build-ups in the mini-basins generated by the topography of the MTD upper surfaces.